THIS MONTH IN

JNM

PET and hypoxia: Carlin and Humm review current understanding of the physiologic processes underlying hypoxia and its imaging with PET tracers and offer perspectives on future directions in clinical utility in diagnosis and treatment management. . . . . ***Page 1171***

^{18}F-NaF kinetics and reproducibility: Kurdziel and colleagues evaluate the kinetics of ^{18}F-sodium fluoride and reassess recommended dose, optimal uptake period, and reproducibility using a current-generation PET/CT scanner . . . . . ***Page 1175***

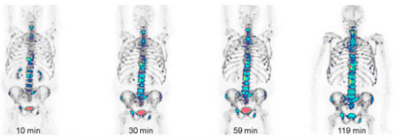

Pretargeted RIT in MTC: Salaun and colleagues describe a phase II trial of the efficacy and safety of anti–carcinoembryonic antigen pretargeted radioimmunotherapy in patients with metastatic medullary thyroid carcinoma, including correlation of serum biomarkers with outcomes . . . . . ***Page 1185***

Reproducibility of lymphoscintigraphy: Vidal and colleagues compare results of lymphoscintigraphy performed by different team members following a strict protocol to assess lymphatic drainage and location and number of sentinel lymph nodes in patients with melanoma. . . . . ***Page 1193***

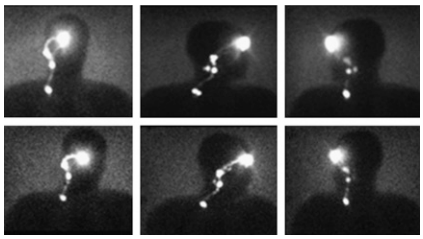

PET/CT in esthesioneuroblastoma: Broski and colleagues explore the clinical utility of ^{18}F-FDG PET/CT in staging and restaging of this rare nasal cavity cancer and quantify the incremental benefit of PET/CT to conventional imaging . . . . . ***Page 1200***

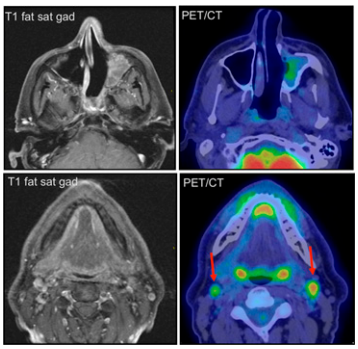

^{64}Cu-DOTATATE and neuroendocrine tumors: Pfeifer and colleagues detail first-in-humans PET/CT use of this avidly binding somatostatin receptor ligand in patients with a history of neuroendocrine tumors and compare results with those from ^{111}In-DTPA-octreotide SPECT/CT. . . . . ***Page 1207***

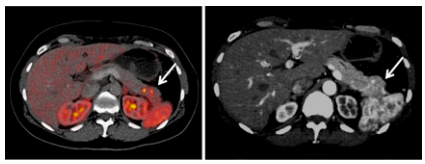

Calcification and myocardial ischemia: Yamazato and colleagues use adenosine stress myocardial perfusion SPECT to investigate the hypothesis that aortic valve calcification is strongly associated with inducible myocardial ischemia, even among asymptomatic patients . . . . . ***Page 1216***

Vulnerable folate–FITC plaque imaging: Jager and colleagues conjugate the ligand folate with fluorescein isothiocyanate to research the potential of folate receptor β fluorescence imaging in identifying vulnerable sites of macrophage accumulation in atherosclerotic plaque . . . . ***Page 1222***

MFR in ^{13}N-ammonia PET: Fiechter and colleagues evaluate the added diagnostic value of myocardial flow reserve over conventional nuclear myocardial perfusion imaging alone as assessed by ^{13}N-ammonia PET/CT to predict angiographic coronary artery disease . . . . . ***Page 1230***

SPECT/CT in infectious endocarditis: Erba and colleagues look at the value of ^{99m}Tc-HMPAO white blood cell scintigraphy, including SPECT/CT acquisitions, in patients with suspected infectious endocarditis . . . . . ***Page 1235***

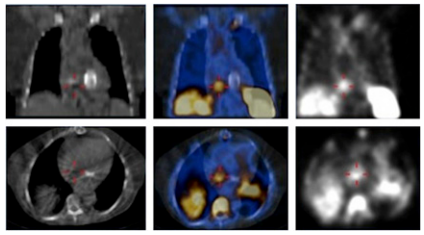

PET/MRI in oncology: Buchbender and colleagues continue their educational overview of integrated PET/MRI in oncologic applications with a review of current literature on utility in tumors of the bone, soft-tissue sarcoma, melanoma, and lymphoma. . . . . ***Page 1244***

PET tracer selectivity: Wiriyasermkul and colleagues examine the interaction of PET tracer ^{18}F-α-methyl tyrosine with L-type amino acid transporter 1 to elucidate mechanisms of tracer uptake in tumors. . . . . ***Page 1253***

^{18}F-tracer uptake and microenvironment: Huang and colleagues compare intratumoral

accumulation of ^{18}F-labeled FDG, fluorothymidine, and misonidazole and relate the results to specific components of tumor microenvironment in mouse models of human non–small cell lung cancer . . . . . ***Page 1262***

PET in multiple sclerosis animal model: Buck and colleagues describe efforts to establish an MRI- and PET/CT-based approach for in vivo definition of multiple sclerosis lesions and to evaluate promising PET tracers in the animal model of experimental autoimmune encephalomyelitis . . . . . ***Page 1269***

Novel ^{99m}Tc-labeled renal tracer: Lipowska and colleagues detail the development of a new renal tricarbonyl radiotracer based on the aspartic-*N*-monoacetic acid ligand and compare experimental pharmacokinetics with those of ^{131}I-*ortho*-iodohippurate . . . . . ***Page 1277***

MRI-based motion correction for PET/MRI: Chun and colleagues present an approach to respiratory motion correction using simultaneous PET/MRI in phantoms, rabbits, and nonhuman primates and discuss prospects for routine clinical use . . . . . ***Page 1284***

Fast spiral SPECT: Vaissier and colleagues describe development and testing of spiral trajectories of the small-animal SPECT bed with a stationary γ-camera and focusing pinholes to improve temporal resolution and reduce image reconstruction times . . . . . ***Page 1292***

NEMA NU 4-2008 comparison: Goertzen and colleagues review performance standards data from the National Electrical Manufacturers Association on a collection of commercial small-animal PET systems manufactured since 2000 . . . . . ***Page 1300***

MIRD and quantitative SPECT: Dewaraja and colleagues present an overview of 3-dimensional SPECT methods and requirements for patient-specific internal radionuclide therapy dosimetry at both regional and voxel levels and introduce an upcoming series of MIRD pamphlets. . . . . ***Page 1310***

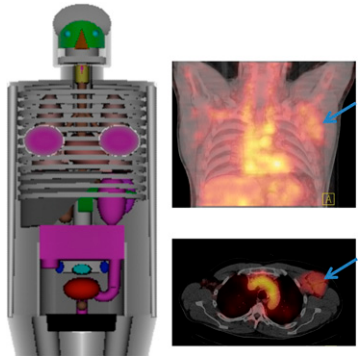

ON THE COVER

Respiratory and cardiac motion is the most serious limitation to whole-body PET. Here, reconstructed PET images of a freely breathing monkey show that MRI-based motion correction in simultaneous PET/MRI increases contrast and resolution but does not increase noise. This results in significant improvement in PET image quality and is a compelling rationale for further evaluation in clinical studies.

See page 1291.